Mon. Not. R. Astron. Soc. **000**, 1–12; (2008) Printed 1 December 2008 (MN LATEX style file v2.2)

Radio source stacking and the infrared / radio correlation at microJy flux densities

Timothy Garn[1,2⋆] and Paul Alexander[2]
[1]*SUPA, Institute for Astronomy, Royal Observatory Edinburgh, Blackford Hill, Edinburgh EH9 3HJ*
[2]*Astrophysics Group, Cavendish Laboratory, 19 J. J. Thomson Ave., Cambridge CB3 0HE*

1 December 2008

ABSTRACT
We investigate the infrared / radio correlation using the technique of source stacking, in order to probe the average properties of radio sources that are too faint to be detected individually. We compare the two methods used in the literature to stack sources, and demonstrate that the creation of stacked images leads to a loss of information. We stack infrared sources in the *Spitzer* extragalactic First Look Survey (xFLS) field, and the three northern *Spitzer* Wide-area Infrared Extragalactic survey (SWIRE) fields, using radio surveys created at 610 MHz and 1.4 GHz, and find a variation in the absolute strength of the correlation between the xFLS and SWIRE regions, but no evidence for significant evolution in the correlation over the 24-μm flux density range 150 μJy – 2 mJy. We carry out the first radio source stacking experiment using 70-μm-selected galaxies, and find no evidence for significant evolution over the 70-μm flux density range 10 mJy – 100 mJy.

Key words: infrared: galaxies — radio continuum: galaxies

1 INTRODUCTION

There is a well-known relationship between the infrared and radio flux densities of star-forming galaxies (the 'infrared / radio correlation', e.g. Helou, Soifer & Rowan-Robinson 1985; Appleton et al., 2004) that is thought to be the result of both the infrared and radio emission from star-forming galaxies being related to the rate of massive star formation. Recent studies of the infrared / radio correlation within nearby galaxies (e.g. Murphy et al. 2006) give weight to this argument, as the radio emission has been shown to represent a smeared out version of the infrared emission. This has been attributed to the diffusion of cosmic ray electrons away from star-forming regions. The correlation is seen to apply to a wide range of galaxies associated with star-formation, but not to those sources which are associated with Active Galactic Nuclei (AGN) activity (e.g. de Jong et al. 1985; Sanders et al. 1988; Sopp & Alexander 1991; Roy et al. 1998).

Studies at high redshift are tentatively finding that the infrared / radio correlation does not deviate significantly from that seen in the local Universe, at least out to $z \sim 1$ (e.g. Garrett 2002; Appleton et al. 2004; Frayer et al. 2006), and potentially to $z \sim 3.5$ (Ibar et al. 2008). The correlation has been shown to remain invariant over more than 5 orders of magnitude (e.g. Yun, Reddy & Condon 2001), however studies that rely on samples of sources which are detected at both infrared and radio wavelengths will naturally be mainly sampling luminous galaxies, and there has been relatively little work carried out on testing the infrared / radio correlation within fainter galaxies.

The technique of source 'stacking' is well established as a method for combining data from many individual objects in order to study the statistical properties of sources which would otherwise be below the detection limit for a particular survey. By constructing a list of source positions based on prior information obtained at another frequency, a series of small 'cut-out' images can be created, centred on these source positions, of sources that may be below the noise level (and therefore undetected). If N of these images are combined, each with a local noise of σ, then the noise level of the stacked image will be expected to decrease approximately as $\sigma/\sqrt{N}$, which quickly allows sources below the original detection threshold of the survey to be studied. Stacking has previously been carried out using optical (e.g. Zibetti et al. 2005) and infrared (e.g. Zheng et al. 2006, 2007) images, as well as in the radio. The large coverage area of the Faint Images of the Radio Sky at Twenty-cm (FIRST; Becker, White & Helfand 1995) survey has led to a number of stacking experiments being carried out (e.g. Wals et al. 2005; de Vries et al. 2007; White et al. 2007; Hodge et al. 2008), looking at the radio properties of quasars and LL-AGN, and some studies of star-forming galaxies have taken place using smaller, but deeper radio surveys (e.g. Boyle et al. 2007; Ivison et al. 2007; Beswick et al. 2008; Carilli et al. 2008).

There have been two stacking studies of the infrared / radio correlation for galaxies which are detected in the infrared, but are below the detection limits of their radio surveys. The strength of the infrared / radio correlation can be quantified by the logarithmic flux density ratio q_{24} (Appleton et al. 2004, and see Sec-

⋆ E-mail: tsg@roe.ac.uk

Table 1. A summary of the properties of the radio surveys used in this work. The area and resolution of each survey, and the noise level at the centre of each image are given, along with the primary reference paper, which should be consulted for further details.

Field	Instrument	Frequency	Area (deg^2)	Resolution ($arcsec^2$)	Position Angle (deg)	Noise level (μJy beam^{-1})	Reference
xFLS	VLA	1.4 GHz	4	5.0×5.0	0	23	Condon et al. (2003)
xFLS	GMRT	610 MHz	4	5.8×4.7	60	30	Garn et al. (2007)
ELAIS-N1	GMRT	610 MHz	9	6.0×5.0	45	40 / 70[a]	Garn et al. (2008a)
Lockman Hole	GMRT	610 MHz	5	6.0×5.0	45	60	Garn et al. (2008b)
ELAIS-N2	GMRT	610 MHz	6	6.5×5.0	70	90	Garn et al. (2009)

[a] Deep / shallow regions respectively.

tion 2.3), and the results from these studies appear to be inconsistent, with Boyle et al. (2007) finding a significantly higher value of q_{24} than is observed in sources which are detected in both wavebands, and Beswick et al. (2008) finding a significantly lower value of q_{24}, and a tentative evolution in the value of q_{24} with 24-μm flux density. In this work we describe a stacking study of the infrared / radio correlation, using the sensitive *Spitzer Space Telescope* (Werner et al. 2004) observations of the *Spitzer* extragalactic First Look Survey field (xFLS) and the *Spitzer* Wide-area Infrared Extragalactic survey (SWIRE; Lonsdale et al. 2003) fields. The three northern SWIRE fields are the European Large-Area *ISO* Survey-North 1 (ELAIS-N1), -North 2 (ELAIS-N2) and Lockman Hole regions, and we take radio data from a 1.4-GHz Very Large Array (VLA) survey of the xFLS field (Condon et al. 2003), and 610-MHz Giant Metrewave Radio Telescope (GMRT) surveys of the xFLS (Garn et al. 2007), ELAIS-N1 (Garn et al. 2008a), Lockman Hole (Garn et al. 2008b) and ELAIS-N2 (Garn et al. 2009, in prep.) regions.

In Section 2 we describe the two stacking techniques which are used in the literature, and calculate the values of q_{24}, using 1.4-GHz data from within the xFLS field. In Section 3 we extend this work to the four 610-MHz survey fields, and demonstrate that AGN contamination is not a significant problem for our infrared samples. We compare the results from our four fields in Section 4, and find a field-to-field variation in the infrared / radio correlation, which is too great to be explained through cosmic variance. We compare our results to those of Boyle et al. (2007) and Beswick et al. (2008), and discuss potential explanations for the systematic variation.

2 STACKING TECHNIQUES

Previous stacking studies of the infrared / radio correlation have been carried out at 1.4 GHz, and in order to compare our results to those in the literature we initially stack infrared sources within the xFLS field using the 1.4-GHz image of the region (Condon et al. 2003). A summary of the characteristics of this survey, and the other radio surveys used in this work, is given in Table 1. Positional information for the infrared sources was taken from the 24-μm source catalogue of Fadda et al. (2006), which contains 16,905 extragalactic point sources above a signal-to-noise (S/N) of 5. The source catalogue is 50 per cent complete over the field at a 24-μm flux density of 300 μJy, with a flux density limit of 210 μJy, while a deeper verification region, covering approximately 10 per cent of the field, is 50 per cent complete to 150 μJy, with a flux density limit of 120 μJy.

Of the 16,905 sources in the catalogue, 14,820 are located within the 1.4-GHz image. A small (~ 0.1 arcsec) positional offset between the 24 μm catalogue and the radio image was identified and removed before performing any stacking. The xFLS 24-μm catalogue does not classify sources by type, however we will demonstrate in Section 3.2 that there is no significant contamination in the catalogue from stars or AGN. There are two principal methods used in the literature to carry out stacking experiments, which are described in Sections 2.1 and 2.2.

2.1 Measuring the flux density of individual sources

The first method for carrying out source stacking measures the radio flux density at each of the individual source positions, bins the sources by their infrared flux density, and uses the statistical distribution of radio flux density for sources within an infrared flux density bin to calculate the typical source properties. While the individual measurements will be very uncertain, particularly for sources near to, or below the noise level, the statistical properties of the distribution should be robust (e.g. White et al. 2007).

The resolution of the 1.4-GHz xFLS image is 5×5 arcsec^2. In order to calibrate the flux density measurements, a circular aperture with radius of 4 arcsec was centred on the location of 79 moderately bright radio sources, and the total flux density within the aperture measured. An aperture correction factor was then calculated, in order to match the measured flux densities of the bright sources to their catalogued values (Condon et al. 2003). Any errors in flux density measurement will propagate through the remainder of the analysis, so the sources that were used for this calibration were required to be:

(i) Brighter than 1 mJy total flux density, so that sources were detected with high significance and the catalogued flux density measurements were known to be accurate.

(ii) Fainter than 10 mJy total flux density. This requirement is very important when calibrating the aperture size for the GMRT images in later sections, since > 10 mJy sources can be strongly affected by phase errors (e.g. Garn et al. 2008a).

(iii) Within the central region of the mosaic, so that any edge effects and increasing noise levels due to the varying primary beam would not affect the flux density calibration.

(iv) Unresolved, with a ratio of total to peak flux density $<$ 1.5. The faint star-forming galaxies being stacked are expected to be unresolved, with a typical size of ~ 1.5 arcsec (Beswick et al. 2008) and a stacking analysis would not be appropriate for extended sources due to the different flux density distribution for each object.

The calculated correction factor for a 4-arcsec aperture was 1.37 for the VLA xFLS image (with similar values found for the four GMRT images which are used later in this work). This correction factor has been calculated only from sources with flux densities between 1 and 10 mJy, and may not be appropriate for fainter radio sources – if this is the case, then varying the aperture size (and hence the correction factor) will lead to different results. We tested aperture sizes between 2 and 10 arcsec – after applying the correction factor, the flux density measurements for the faint sources were consistent with each other for aperture sizes between 2 and 5 arcsec. At greater sizes, the radio flux density calculated for the faint sources began to increase. We used a 4 arcsec radius aperture for all stacking measurements described in this work, and all measurements made within the aperture have had the correction factor applied unless otherwise stated.

The flux density measurement technique described in this section sums all of the radio flux density within a circular aperture, irrespective of its origin. There is the possibility that a 4 arcsec radius aperture is sufficiently large that source confusion may be a problem (where the radio emission from more than one source is incorrectly assumed to all result from a single 24-μm target). In order to test for source confusion, we used the *Spitzer* Infrared Array Camera (IRAC; Fazio et al. 2004) observations of the xFLS field to identify nearby counterparts to the 24-μm sources. The IRAC source catalogue (Lacy et al. 2005) contains 103,193 sources with detections in at least one of the 3.6-, 4.5-, 5.8- and 8-μm bands.

We selected a sample of 9062 24-μm sources which were located within the centre of the IRAC observations, and measured the number of IRAC counterparts within 4 arcsec of each 24-μm source. While some of the 24-μm sources do not have an IRAC counterpart (917; 10.1 per cent), the majority of the sources had a single IRAC counterpart within 4 arcsec (7712; 85.1 per cent), with only 409 sources (4.5 per cent) having two counterparts and 24 sources (0.3 per cent) having three. We conclude that confusion from nearby faint sources will not significantly affect the radio flux density measurements.

Fig. 1(a) shows the measured (aperture-corrected) 1.4-GHz radio flux densities for each source in the 24-μm catalogue, along with $\pm 4\sigma$ (where 4σ is the detection limit for individual radio sources). The figure is plotted on a log-linear scale in order to show the range of radio flux density that is measured, which can be negative due to the effects of noise. The decreased number of sources in Fig. 1 (and later figures displaying xFLS data) which have a 24-μm flux density of < 300 μJy is due to the smaller coverage area of the deep verification region of the survey.

In order to look at the statistical properties of sources, we bin them logarithmically by their 24-μm flux densities, and calculate the median infrared and radio flux density in each bin. The median estimator is more robust to outliers than the mean, and we will demonstrate that the median is the most appropriate choice for this data in Section 2.2. We plot the median binned flux densities in Fig. 1(a), with distribution widths which denote the inter-quartile range (IQR) for each bin, a more robust measurement of the range than the standard deviation.

For comparison, Fig. 1(b) shows the measured radio flux densities from 14,820 random source positions in the image – a few locations have a measured flux density above the 4σ detection limit and appear to have a source present, but the remainder of the random positions have measured flux density below the detection threshold. The median radio flux density for all bins is consistent with zero.

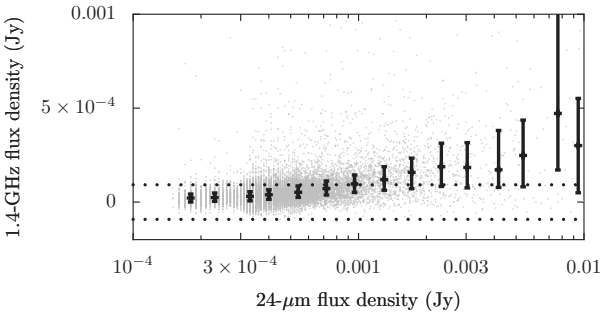

(a) Measured and median binned radio flux density for the 14,820 24-μm sources within the xFLS 1.4-GHz image of Condon et al. (2003). Note that the majority of sources are below the limit at which they could be detected individually, as shown by the upper dotted line, and would not be included in a conventional analysis.

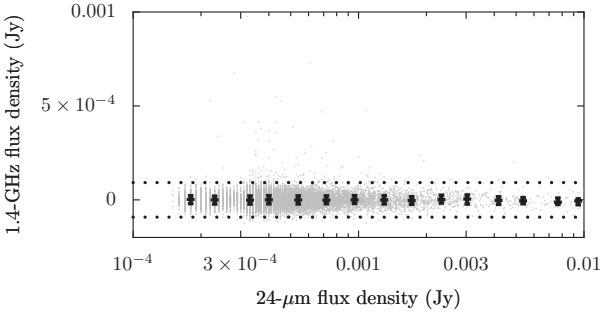

(b) Measured and median binned radio flux density for 14,820 random source positions, with each position assigned a 24-μm flux density from the catalogue at random. The radio flux density in each bin is consistent with zero.

Figure 1. The 1.4-GHz radio flux density for each source in the 24-μm catalogue, measured as described in Section 2.1 (grey dots), the values of $\pm 4\sigma$ (horizontal black dotted lines) and the median values of flux density within each bin (black points with errors). The error bars denote the size of the IQR of radio flux density in each bin. The vertical striping seen in this and later figures is an artefact of the quoted precision of the 24-μm catalogue. The decrease in the number of sources seen below a 24-μm flux density of 300 μJy is due to the smaller coverage area of the verification region – see text for more details.

2.2 Creating stacked images

The second method used in the literature to measure the flux density of sources via stacking is to create a 'stacked image' that is representative of the average properties of sources within each infrared flux density bin, and then calculate the radio flux density directly from that image. Small 'cut-out' images are generated, centred on each source within a flux density bin, and the value of each pixel in the stacked image calculated from the mean or median of the distribution of flux density that is seen from the equivalent pixels in the N cut-out images.

In order to compare this technique to the one described in Section 2.1, we create 41×41 pixel^2 (61.5×61.5 arcsec^2) cut-out images which are centred on each of the 24-μm sources within the xFLS field, and create mean and median stacked images, using the same bins as in Section 2.1. The noise of the median stacked images was calculated using SOURCE EXTRACTOR (Bertin & Arnouts 1996), and is a good fit to a $1/\sqrt{N}$ relationship, although with an initial noise level of 26 μJy beam^{-1}, 13 per cent larger than the value of 23 μJy beam^{-1} quoted by Condon et al. (2003). The bin containing the most sources has a noise level of

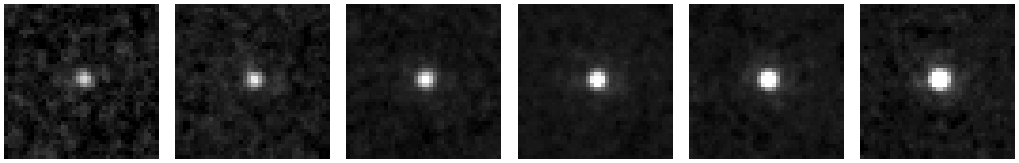

(a) 150 – 201 μJy. (b) 201 – 268 μJy. (c) 268 – 359 μJy. (d) 359 – 479 μJy. (e) 479 – 641 μJy. (f) 641 – 857 μJy.

Figure 2. Median stacked 1.4-GHz radio images for the faintest six flux density bins. All images have a size of 61.5×61.5 arcsec^2 (41×41 pixel^2). The 24-μm flux density range of sources used to create the stacked image are given below each sub-image, with further details in Table 2. The grey-scale ranges between -2 and 20 μJy beam^{-1}.

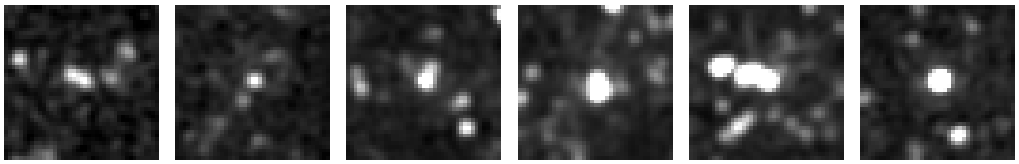

(a) 150 – 201 μJy. (b) 201 – 268 μJy. (c) 268 – 359 μJy. (d) 359 – 479 μJy. (e) 479 – 641 μJy. (f) 641 – 857 μJy.

Figure 3. Mean stacked 1.4-GHz radio images for the same 24-μm flux density bins shown in Fig. 2. As in Fig. 2, images are 61.5×61.5 arcsec^2 and the grey-scale ranges between -2 and 20 μJy beam^{-1}, but the presence of a few bright sources in each stacked image make the resultant mean images no longer representative of the 'typical' sources within a flux density bin.

Table 2. The infrared flux density range, number of sources in each bin N, median value of 1.4-GHz flux density $S_{1.4}$ and the noise level σ for the six median stacked images shown in Fig. 2.

Bin	S_{24} (μJy)	N	$S_{1.4}$ (μJy)	σ (μJy beam^{-1})
1	150 – 201	466	21.2	1.21
2	201 – 268	855	25.2	0.80
3	268 – 359	2565	30.5	0.59
4	359 – 479	4583	39.0	0.42
5	479 – 641	2795	53.7	0.49
6	641 – 857	1476	72.2	0.64

424 nJy beam^{-1}, more than 50 times lower than the noise level of the VLA xFLS image, and $\sim$ ten times lower than the most sensitive VLA observations to date.

In Fig. 2 we show the median stacked images created for the six faintest bins, along with the range of 24-μm flux density that the bin covers. The number of sources in each bin, the total flux density of the stacked source and the noise level of the stacked image are listed in Table 2. There is a clearly-visible point source seen in each image, with a circular appearance given by the 5×5 arcsec^2 resolution of the original VLA mosaic. In contrast to this, Fig. 3 shows the mean stacked images for the same six bins. All images are noticeably noisier than their median equivalents, and bright sources away from the centre of the cut-out images have a much greater effect on the stacked images. The noise level of the mean images is $\sim 1.5 - 3$ times the noise of the median images, and the mean images are not representative of the typical sources within each flux density bin, but are strongly biased by a few bright radio sources.

We calculated the radio flux density of the stacked images, and compared the results to the median radio flux density in each bin as calculated in Section 2.1. The median results are in good agreement with each other, as is expected for point sources and a Gaussian noise distribution – the flux density measured from the median image is equivalent to the median of the flux densities measured from the individual images. While the two methods for estimating the median radio flux density give equivalent results, creating stacked images means that the information on the IQR of the flux density distribution is discarded. We therefore use the median binned flux density within an aperture for all future flux density measurements in this work.

2.3 Calculating median values of q_{24}

The infrared / radio correlation can be quantified through the logarithmic flux density ratio $q_{\rm IR}$ (Appleton et al. 2004), where

$$q_{\rm IR} = \log_{10}\left(\frac{S_{\rm IR}}{S_{1.4}}\right), \quad (1)$$

and $S_{\rm IR}$ is the infrared flux density detected within either the *Spitzer* 24-μm or 70-μm bands. In Fig. 4(a) the value of q_{24} for each source in the 24-μm catalogue is shown, along with the 'median binned' value of q_{24}, which is calculated directly from the median values of infrared and radio flux density within each flux density bin. The error bars on q_{24} come from the radio flux density at the IQR for each flux density bin, and therefore represent the same range as was shown in Fig. 1. Since sources with an apparent value of radio flux density that is negative (of which there are many – see Fig. 1) cannot be plotted on this figure, the median value of q_{24} does not follow the trend of the individual plotted points directly – this can be seen by the asymmetric distribution range for the fainter flux density bins.

Appleton et al. (2004) carried out the first study of the infrared / radio correlation in the xFLS field, using a 1.4-GHz radio catalogue (Condon et al. 2003), and early 24-μm *Spitzer* data. 508 sources were found with both 24-μm and 1.4-GHz detections. Appleton et al. (2004) calculated a mean value of $q_{24} = 0.84 \pm 0.28$ for these sources, which is shown on Fig. 4(a) for comparison with our data. Note that the initial survey data which has been used for both the Appleton et al. (2004) study and the study described in this section is the same. It is clear that our stacking results give a value of q_{24} that is greater than the Appleton et al. (2004) mean value

(i.e. we find that sources are more radio-quiet than was found by Appleton et al. 2004), which is to be expected due to the fact that the Appleton et al. (2004) sample contained only those sources detected at both frequencies, and is therefore subject to significant sample bias.

In order to test the effects of this bias, we created a catalogue of 1.4-GHz radio sources in the xFLS field, using the method described in Garn et al. (2007), and requiring that sources could be detected at the 4σ level. We then repeated the stacking experiment described above, using only the 2,558 24-μm sources which were also present in this 1.4-GHz catalogue. Fig. 4(b) shows the individual values of q_{24} for each source, calculated using the method described in Section 2.1, along with the median binned values of q_{24}. The 4σ limit is shown on this plot, although some sources have a measured flux density below this limit (i.e. a value of q_{24} above the dashed line) due to the effects of noise on the aperture flux density measurements. An artificial variation of q_{24} with infrared flux density is now seen, although this is purely a selection effect and clearly demonstrates the disadvantage of only studying the bright sources which can be detected in radio images. Now that the median values of q_{24} are being calculated from sources that can be clearly seen above the noise, the binned data follows the trend of individual sources and the flux density distribution is both narrower and more symmetric.

A comparison of the Appleton et al. (2004) results and the binned data from detected sources in Fig. 4(b) shows good agreement, with the binned results spanning the width of the distribution found by Appleton et al. (2004). This suggests that the stacking method is not significantly biasing the radio flux density which is measured for sources. We overlay the values of q_{24} found in the stacking experiments of Boyle et al. (2007) and Beswick et al. (2008) on Fig. 4 for comparison with our data. Note that the Beswick et al. (2008) results are not suffering from the selection effect which was described above, resulting from only using detected sources, despite appearing to follow a similar trend to our binned data in Fig. 4(b) – 80 per cent of their infrared sources can be detected above 3σ in their radio image, and all sources have been used for the stacking experiment (see Section 4.6 for further details). All three stacking experiments find very different values for q_{24}, with the sources in the study of Boyle et al. (2007) being more radio-quiet than our data, and the sources in the Beswick et al. (2008) study being more radio-loud. A detailed comparison of our results with those of Boyle et al. (2007) and Beswick et al. (2008) will be performed in later sections.

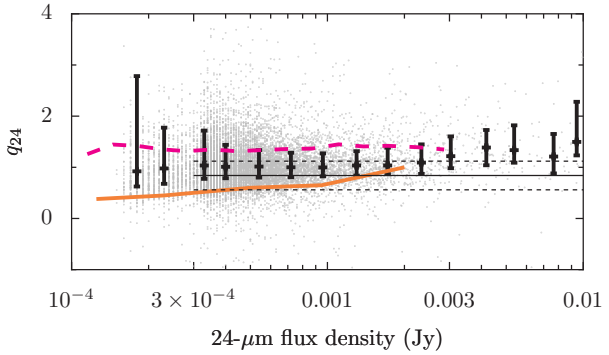

(a) q_{24}, calculated from all 14,820 sources in the 24-μm catalogue. There is no significant variation in the median value of q_{24} over the range of S_{24} plotted.

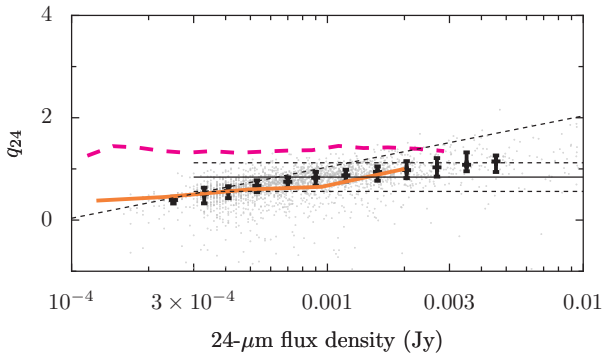

(b) q_{24}, calculated only from the 2,558 sources that are also detected above 4σ at 1.4-GHz. The median value of q_{24} follows the trend of individual sources. The diagonal dashed line represents a constant radio flux density of 4×23 μJy. Bins containing fewer than 20 sources have been excluded from the figure.

Figure 4. The effects of varying the selection criteria when calculating q_{24}. Values of q_{24} for individual sources are shown (grey dots), along with the median binned value of q_{24} (black points with errors denoting the IQR of the data). Note that sources with an apparent radio flux density < 0 cannot be shown on these plots. The decrease in the number of sources seen below a 24-μm flux density of 300 μJy is due to the smaller coverage area of the verification survey – see Section 2 for more details. The values of q_{24} found in the stacking experiments of Boyle et al. (2007) (thick pink dashed line; CDFS field only, 'all-source' data – see Section 4.5 for further details) and Beswick et al. (2008) (thick orange solid line) are plotted for comparison. The horizontal black lines represent the mean value of q_{24} of 0.84 ± 0.28 found by Appleton et al. (2004) – see text for more details.

3 610-MHZ STACKING

3.1 *Spitzer* extragalactic First Look Survey field

The strength of the infrared / radio correlation can be quantified at 610 MHz in a similar way to at 1.4 GHz, using

$$q'_{\rm IR} = \log_{10}\left(\frac{S_{\rm IR}}{S_{610}}\right), \qquad (2)$$

where S_{610} is the radio flux density measured at 610 MHz. There are 13,812 24-μm sources located within the region covered by the 610-MHz GMRT image of the xFLS field (Garn et al. 2007). While the noise level of the 1.4-GHz image is fairly uniform across the field, the GMRT image shows more variation (see Fig. 1 of Garn et al. 2007). In order to test whether this varying noise affects the calculated values of q'_{24} we carried out the stacking procedure described in Section 2.1 on the GMRT image, using only those sources within a radius of 25 arcmin from the centre of the mosaic. This analysis was repeated in 12.5 arcmin increments up to 1.25 deg – increasing the radius had no significant effect on the median values of q'_{24}, indicating that the varying noise level within this image was not affecting the results.

We varied the aperture size, and verified that a 4 arcsec aperture was still appropriate for the GMRT image. Fig. 5(a) shows the 610-MHz flux density measured for each source, and the median binned values, for comparison to Fig. 1(a). Due to the increased and varying noise level across the 610-MHz image, there is a greater dispersion in the individual values of flux density being measured, and the IQR of radio flux density for each bin is larger. This is more clearly seen in Fig. 5(b), where the flux density measured at 13,812 random source positions is plotted – since the noise level is not uniform, the individual flux density measurements do not lie as tightly inside the $\pm 4\sigma$ lines as before (where $\sigma = 30$ μJy beam^{-1}, the

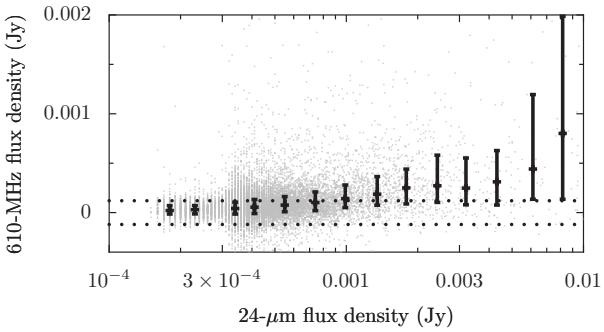

(a) Measured and median binned radio flux density for the 13,812 24-μm sources within the xFLS 610-MHz image.

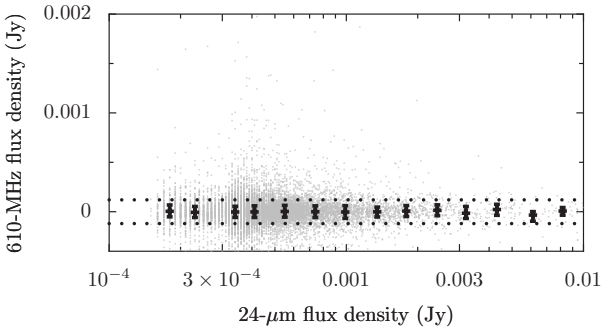

(b) Measured and median binned radio flux density for 13,812 random source positions, with each position assigned a 24-μm flux density from the catalogue at random. The radio flux density in each bin is consistent with zero.

Figure 5. The 610-MHz radio flux density for each source in the 24-μm catalogue, measured as in Section 2.1 (grey dots), the values of $\pm 4\sigma$ (horizontal black dotted lines) for the central region of the image, and the median values of flux density within each bin (black points with errors). The error bars denote the size of the IQR of radio flux density in each bin. The decrease in the number of sources seen below a 24-μm flux density of 300 μJy is due to the smaller coverage area of the verification survey – see Section 2 for more details.

noise at the centre of the 610-MHz image). The median of the distribution is again consistent with having zero flux density in each bin.

3.2 Stacking by source type in the SWIRE fields

We have carried out no selection by source type so far in this work, and have been stacking *all* 24-μm sources together, rather than just those specifically associated with star formation. The 24-μm xFLS catalogue of Fadda et al. (2004) does not classify sources by type, and it is possible that there may be a significant number of stars or AGN in the sample, potentially affecting conclusions that are being drawn for the star-forming galaxy population. At 30 mJy the contribution of stars and galaxies to the 24-μm source counts is roughly the same, but galaxies rapidly dominate below this flux density, and stars do not make up a significant fraction of the source counts over the 24-μm flux density range that we are considering (Shupe et al. 2008).

We carried out source stacking in the three northern SWIRE fields, using the GMRT 610-MHz images of the ELAIS-N1 (Garn et al. 2008a), Lockman Hole (Garn et al. 2008b) and ELAIS-N2 (Garn et al. 2009) fields, and obtaining positional information on infrared sources from the photometric redshift catalogue of

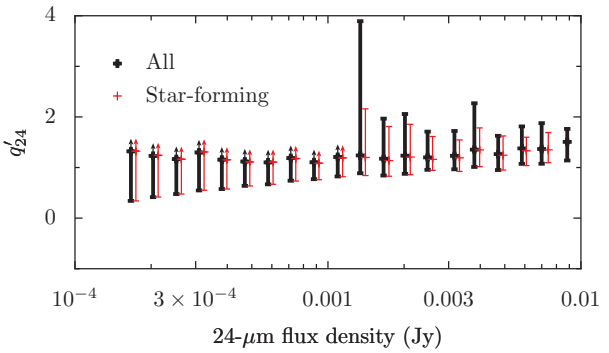

Figure 6. Median values of q'_{24} for sources within the ELAIS-N1 field, along with the IQR of the data. All sources from the Rowan-Robinson et al. (2008) photometric catalogue are shown (thick black points), compared with sources that have been classified as star-forming (thin red points). The star-forming sources have been displaced by a small amount along the x-axis for clarity, but would otherwise lie directly on top of the median value calculated from all sources. No significant difference is seen between the two median values, although the distribution width is smaller for the star-forming sources, demonstrating that AGN contamination increases the uncertainty of the results.

Rowan-Robinson et al. (2008). While the photometric catalogue is not completely unbiased, due to the selection requirements and the need for sufficient photometry to estimate redshifts, all sources within the catalogue have been classified as either galaxies or AGN (with no stars being present). The possibility that the xFLS sample is contaminated by significant numbers of sources that are not star-forming galaxies can thus be tested.

There are 48,882 entries in the photometric catalogue with 24-μm flux densities between 150 μJy and 10 mJy, within the region covered by the ELAIS-N1 image. Of these sources, 2,236 (4.6 per cent) have been classified as fitting AGN templates through their optical and infrared photometry, although no information is available as to which sources may have a significant amount of their radio emission resulting from an AGN, but are not identified as such in the infrared. Fig. 6 shows a comparison between q'_{24} calculated from all sources within the ELAIS-N1 field, and q'_{24} from just those sources classified as star-forming. No significant difference is seen in the median value, with the values for the star-forming sources lying on top of the median values found when using all sources in the catalogue. The IQR decreases when only star-forming sources are used, demonstrating that the AGN sources increase the dispersion in the data, but that the median is resistant to the presence of a small percentage of outliers. The greater noise level for the ELAIS-N1 survey compared with the xFLS 610-MHz survey (~ 70 μJy beam^{-1} across the majority of the image; Garn et al. 2008a) means that the IQR can permit negative radio flux densities for some of the fainter infrared flux density bins – where this occurs, lower limits are shown for the IQR of q'_{24} in Fig. 6.

Repeating this test on the other two SWIRE fields, similar results were found. The presence of known AGN sources in the sample has very little effect on the stacking results, and we conclude that contamination from AGN sources in the xFLS sample will be unimportant. However, all future stacking within the SWIRE fields will use only those 24-μm sources identified as star-forming, with 46,646 sources in ELAIS-N1, 32,265 in ELAIS-N2 and 28,042 in the Lockman Hole.

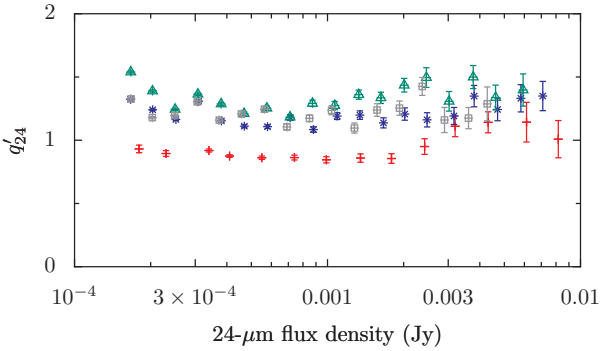

Figure 7. The median values of q'_{24} from the xFLS (red upright crosses) and three SWIRE fields (ELAIS-N1 – blue stars; ELAIS-N2 – green triangles; Lockman Hole – grey squares). The error bars represent the error on the value of the median radio flux density, rather than the IQR.

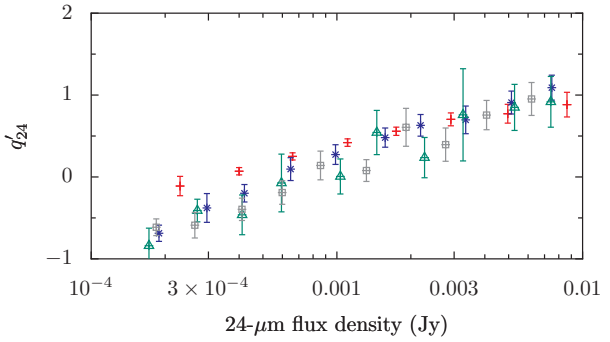

Figure 8. A comparison of q'_{24} for each of the GMRT fields, using the detected radio sources only, with error bars representing the error on the median value of radio flux density. The colour scheme is the same as for Fig. 7. While the varying biases affect the values of q'_{24} found for faint infrared flux densities, no systematic offset is seen between the values of q'_{24} in the four fields for bright sources, in contrast to the result seen in Fig. 7 when all infrared sources are used.

4 DISCUSSION

4.1 SWIRE and xFLS comparison

In Fig. 7 we show the 610-MHz stacking results from the xFLS and SWIRE fields. There is an apparent field-to-field variation seen in the values of q'_{24}, with the xFLS data being systematically lower by ~ 0.3 than the SWIRE data. The offset affects all of the 24-μm flux density bins by approximately the same amount. The error estimates come from the uncertainty in median radio flux density, which scales as $1/\sqrt{N}$ and is equivalent to the error obtained from the noise level of a stacked image. Due to the dependence on $\sqrt{N}$, the fainter flux density bins (which contain many more sources) appear to be much better constrained than the brighter bins, where sources can actually be detected individually.

There are a number of potential explanations for the offset which is seen:

(i) A systematic offset in the flux density calibration in one or more of the radio images (Section 4.2).

(ii) A systematic offset in the flux density calibration in one or more of the infrared catalogues (Section 4.3).

(iii) A bias being introduced into the stacking experiments due to sample incompleteness (Section 4.4).

4.2 Radio flux density calibration

Any systematic flux density calibration offset in the radio surveys would directly translate into a systematic offset in the calculated value of q_{24}. All of the GMRT surveys (Garn et al. 2007, 2008a,b, 2009) were calibrated in the same way, using observations of 3C48 or 3C286. The relative flux density calibration of the xFLS survey is accurate to 7 per cent (Garn et al. 2007), and similar values apply to the three SWIRE survey fields. The effect of a constant calibration error is simple to quantify – if the measured radio flux density $S_{\rm m}$ equals $f\times$ the true flux density $S_{\rm true}$, then the measured value of $q_{\rm m}$ is related to the true value $q_{\rm true}$ via

$$q_{\rm m} = q_{\rm true} - \log_{10}(f). \quad (3)$$

A 7 per cent flux density calibration error would lead to an error in q_{24} of ± 0.03 – ten times too small to account for the difference seen in Fig. 7.

The existence of a systematic calibration offset between the radio surveys can be tested for by considering the only those values of q'_{24} which are calculated from infrared sources with counterparts in the GMRT catalogues from Garn et al. (2007, 2008a,b, 2009). Fig. 8 compares the median values of q'_{24} from each of the GMRT images, using only those detected sources – while the results for faint infrared flux density bins are affected strongly by the same selection effects as were seen in Fig. 4(b), no systematic offset is seen between the median values of q'_{24} for bright infrared sources, in contrast to that seen in Fig. 7. The existence of a systematic offset between the stacked values of q'_{24} in the xFLS and SWIRE fields, which is not seen in the values of q'_{24} calculated from sources which are detected in the radio images, rules out the possibility that the offset is a result of a difference in flux density calibration between the radio surveys. The median value of q'_{24} from bright, detected sources for all fields is ~ 1 in the brightest 24-μm bin, which is in agreement with the value found for the xFLS field using all 24-μm sources.

An error due to the radio flux density calibration can also be ruled out by considering the radio source counts presented in Garn et al. (2008a) – if the xFLS field was systematically brighter than the SWIRE fields, then the 610-MHz differential source counts would be expected to show a systematic offset between the xFLS and SWIRE fields; no such effect was seen. The GMRT source counts also agree with GMRT counts made by other authors, confirming that the relative flux density calibration of the surveys is accurate. It seems unlikely that any large-scale flux density calibration error can be the cause of the discrepancy between the xFLS and SWIRE survey data.

4.3 Infrared flux density calibration

The 24-μm catalogues for the xFLS and SWIRE fields have been created by separate authors (xFLS; Fadda et al. 2004, SWIRE; Rowan-Robinson et al. 2008). While it is equally unlikely that any large-scale flux density calibration error in the infrared could be responsible for the systematic effect which is seen, this can be tested through a stacking experiment in the xFLS and SWIRE fields using 70-μm sources.

There are 601 sources in the Frayer et al. (2006) xFLS catalogue contained within the 610-MHz image, and 1028, 597 and 687 sources from the Surace et al. (2005) SWIRE catalogues within the ELAIS-N1, ELAIS-N2 and Lockman Hole images. We carried out the same stacking procedure, using 70-μm source positions, in or-

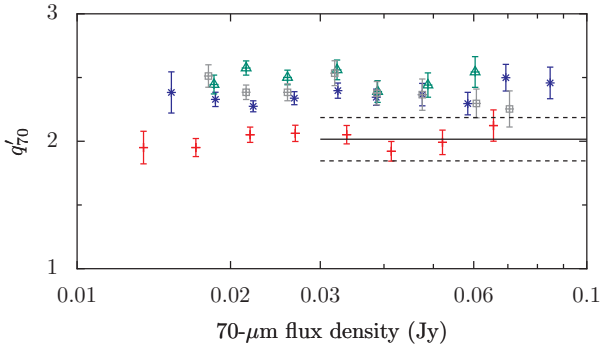

Figure 9. Median values of q'_{70}, along with errors in the median, taken from the four GMRT surveys. The colour scheme is the same as for Fig. 7. The horizontal black lines represent the mean value of $q_{70} = 2.16 \pm 0.17$ found by Appleton et al. (2004), converted to a 610-MHz value using Equation 4 and $\alpha = 0.4$ – see Section 4.4.

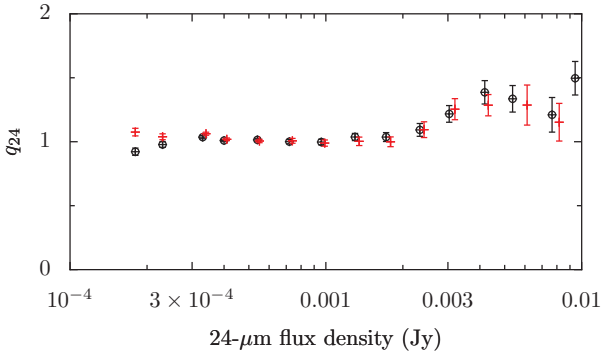

Figure 10. A comparison between q_{24} obtained from the 1.4-GHz image of the xFLS field (black circles) and q'_{24} from the 610-MHz image of the same region, shifted to a 1.4-GHz value through the use of Equation 4 and $\alpha = 0.4$ (red upright crosses). Error bars represent the error on the median value of radio flux density. The shape of the two profiles is consistent across the full range of infrared flux density, ruling out any significant instrument-dependent or data reduction-dependent biases.

der to compare the results to the 24-μm data. Fig. 9 shows the q'_{70} values for the four fields. The error bars on q'_{70} are greater than before, due to the decreased number of sources in the infrared catalogues. The same field-to-field variation is seen, with a similar systematic offset of ~ 0.3 between the xFLS and SWIRE median values of q'_{70}, and no variation in the value of q'_{70} with S_{70} is seen over the range 10 – 100 mJy for any of the survey fields. The similar offset seen in q'_{24} and q'_{70} implies that the offset is not a result of a difference between the Fadda et al. (2004) and Rowan-Robinson et al. (2008) 24-μm catalogues.

We overlay the Appleton et al. (2004) result of $q_{70} = 2.16 \pm 0.17$ on Fig. 9, converted to a 610-MHz value using Equation 4 and $\alpha = 0.4$ (see Section 4.4). The lower sensitivity of the 70-μm data compared with the 24-μm observations (~ 30 mJy compared with ~ 0.3 mJy) makes the sample bias that occurs from only using sources that can be detected in the radio less significant than at 24-μm. As was seen at 24-μm, the Appleton et al. (2004) result agrees well with the xFLS stacking experiment, although our data covers a greater range of 70-μm flux density than Appleton et al. (2004), as the Frayer et al. (2006) source catalogue of the field was not yet available. The good agreement between our stacked q'_{70} values and the Appleton et al. (2004) value is further evidence that the stacking procedure is not significantly biasing the radio flux density measurements.

4.4 Stacking bias

White et al. (2007) carried out a stacking experiment using the FIRST survey, and ran simulations to test how well their stacking experiment could recover the flux density of sources below the noise level. They placed four artificial sources in their *uv* data for each of 400 FIRST observations, and re-reduced the images to fully simulate all of the potential sources of bias that may enter into the data reduction procedure. They found that some of the initial flux density could not be recovered from stacked images, and attribute the loss to an effect equivalent to 'CLEAN bias' (e.g. Becker et al. 1995), despite the fact that sources below the survey threshold *'by definition, have not been CLEANed'* (although see Section 4.5 for a discussion of the stacking simulation carried out by Boyle et al. 2007). However, the second technique that White et al. (2007) used to test for a loss of flux was to take existing deeper observations of an area covered by FIRST (the VLA xFLS survey) to provide positions and flux densities for sources below the FIRST detection threshold, and then stack sources using the prior knowledge of their radio flux density. They found that their stacked images were able to recreate 71 per cent of the true flux density of sources, for all flux density bins. If a constant fraction f of flux is being recovered for all sources, then the required correction factor is also just a constant fraction (in this case 1/0.71 = 1.41) for each infrared flux density bin, rather than varying in a complex manner from source to source. The overall effect of this bias would be to alter the absolute value of q_{24} which is measured, but without changing its dependence on infrared flux density. From Equation 3, the correction factor found by White et al. (2007) would have led to a calculated value which is 0.15 above the true value of q_{24}. In order to obtain an offset of 0.3, the correction factor would have to be $\log_{10}(0.3) \simeq 2$, with only half of the radio flux density of stacked sources being correctly measured.

The linearity of any potential stacking bias can be directly testing within the xFLS field, where the same 24-μm catalogue has been used to stack both 1.4-GHz and 610-MHz sources. Any non-linear form of bias would be expected to affect the two radio images in different ways, due to the separate telescope arrays used to take the observations, the independent data reduction methods, and the different amount of CLEANing. The relationship between q_{24} and q'_{24}, taking a single spectral index α to represent the whole population[1], is

$$q_{24} = q'_{24} - \log_{10}\left(\frac{S_{1.4}}{S_{610}}\right) = q'_{24} + 0.36\alpha. \quad (4)$$

By comparing the binned values of q_{24} and q'_{24} found in the xFLS field, we are able to obtain a single spectral index, $\alpha = 0.4$, which represents the linear shift required to convert between the stacked 610-MHz and 1.4-GHz flux densities. Fig. 10 shows the values of q_{24} calculated from the xFLS 1.4-GHz image, and the values of q'_{24} calculated from the xFLS 610-MHz image, converted to 1.4-GHz values using $\alpha = 0.4$. The shape of the q_{24} and (shifted) q'_{24} data are consistent across the full range of infrared flux density, with the exception of the faintest flux density bin. While the

[1] We define α such that the variation of flux density S_ν with frequency ν is $S_\nu = S_0 \nu^{-\alpha}$.

value of α has been chosen in order to overlay the q_{24} and q'_{24} profiles, making the absolute values shown in Fig. 10 not independent of each other, the consistent shape of the q_{24} and q'_{24} profiles in Fig. 10 demonstrates that any stacking bias which is present must be a simple fraction of the true flux density, as was found by White et al. (2007), and rules out any significant non-linear flux-dependent stacking bias.

4.5 Comparison with the results of Boyle et al. (2007)

The stacking experiment of Boyle et al. (2007) is similar to that presented in this work, also using 24-μm sources detected in the SWIRE survey, in the *Chandra* Deep Field South (CDFS) and ELAIS-S1 fields. The infrared observations of the ELAIS-S1 field were much less sensitive than the CDFS observations, and the results from the two fields were broadly similar, so we only compare our results to those from the CDFS field.

The Boyle et al. (2007) radio data came from a 1.4-GHz Australia Telescope Compact Array (ATCA) survey, with an rms noise level of 30 μJy beam^{-1} and resolution of 11×5 arcsec^2 (Norris et al. 2006). The *Spitzer* catalogue of the CDFS field contains ∼12,000 sources above an infrared 5σ flux density limit of 100 μJy (while the ELAIS-S1 survey only contains ∼2,000 sources above a flux density limit of 400 μJy). Median stacked radio images were created from the binned CDFS sources, and the peak flux density of these images was taken as their estimate of the radio flux density. They select data in two ways – an 'all-source' sample, where all the data was used, and a 'quiet-source' sample, where cut-out images that had a central pixel with radio flux density of > 100 μJy were not used to create the stacked image. Due to the exclusion of visibly-present radio sources, the 'quiet-source' stack suffers from a systematic bias in the brighter flux density bins, and underestimates the radio flux density for the stacked sources (as can be seen in their Fig. 4) – for this reason, all comparisons to Boyle et al. (2007) data in this work are with the 'all-source' sample.

Boyle et al. (2007) found a value of $q_{24} = 1.39$, and no significant variation with S_{24} over the range 100 – 2800 μJy. Fig. 11 shows the values of q_{24} found by Boyle et al. (2007) in the CDFS, and the values of q'_{24} from the three 610-MHz SWIRE fields, converted to 1.4-GHz values using the spectral index of $\alpha = 0.4$ found from the xFLS comparison in Section 4.4. The Boyle et al. (2007) results agree with the general trend of the 610-MHz SWIRE results, although the data in individual flux density bins are not always completely consistent. The errors on the fainter flux density bins from the 610-MHz SWIRE fields are significantly smaller than the Boyle et al. (2007) data, due to the increased number of 24-μm sources present in the Rowan-Robinson et al. (2008) data compared with the earlier Surace et al. (2005) SWIRE catalogues used by Boyle et al. (2007).

Beswick et al. (2008) argued that some of the discrepancy between their results ($q_{24} = 0.48$; see Section 4.6) and those of Boyle et al. (2007) could be due to a systematic under-estimation of the radio flux density by up to a factor of 2 by the ATCA for sources at low flux densities. This would lead to an over-estimation of q_{24} by Boyle et al. (2007) of ~ 0.3, reducing their value to ~ 1.1 in the faint 24-μm flux density bins (and therefore agreeing with our xFLS data). However, our findings are not consistent with this interpretation, with our SWIRE stacking results agreeing with the Boyle et al. (2007) data after using a conversion between 610-MHz and 1.4-GHz results calculated from the xFLS field, independent of the SWIRE data. Norris et al. (2006) found through comparing their radio data to a more sensitive survey of the GOODS-South portion of the region (Afonso et al. 2006) that the ATCA flux densities were only being under-estimated by about 14 per cent, which would lead to an over-estimation of the Boyle et al. (2007) value of q_{24} by ~ 0.07 – this amount of variation is within the typical field-to-field dispersion seen from the three 610-MHz SWIRE surveys, and cannot be ruled out. While any underestimation of ATCA radio flux densities has been shown to be small at high flux density, this effect may be more significant for lower flux density sources – see e.g. Prandoni et al. (2000) – which would affect the faint stacked sources (< 130 μJy) studied by Boyle et al. (2007) more significantly than the brighter discrete objects (> 200 μJy) discussed by Norris et al. (2006). It remains unclear as to the potential size or cause of any systematic underestimation of radio flux densities in ATCA observations.

Boyle et al. (2007) recognized that their value of $q_{24} = 1.39$ was unexpectedly high – '*greater than any modelled SED*', and so carried out simulations to test for any effects such as the stacking bias described in Section 4.4. They inserted sources into their image, and confirmed that they were able to recreate the median value of the source population through the use of stacking. More importantly in the context of this work, they inserted sources into their *uv* data and reprocessed the images to fully simulate all of the effects which could be biasing the stacked flux density values. Their stacking measurements gave them '*an essentially identical result*' to simulations in the image plane, and to their original data, which suggests that any stacking bias in their experiment must be small.

The fact that the same conversion factor which was found for the xFLS data (of $\alpha = 0.4$) also allows the Boyle et al. (2007) and 610-MHz SWIRE data to agree implies that there can be little stacking bias in the 610-MHz surveys. Any significant bias which only applied to the GMRT xFLS image would lead to a value of α which would not be suitable for the SWIRE fields, contrary to what is seen. We do not believe that a stacking bias can be the cause of the observed discrepancy between the xFLS and SWIRE results.

4.6 Comparison with the results of Beswick et al. (2008)

Beswick et al. (2008) performed their stacking experiment on a sample of 377 24-μm sources detected with *Spitzer* in the *Hubble* Deep Field-North (HDF-N), 303 of which can be seen above 3σ in a deep Multi-Element Radio-Linked Interferometer Network (MERLIN) and VLA image of the field with rms noise level of 3.6 μJy beam^{-1} and resolution of 0.4 arcsec. They measured radio flux densities using both of the techniques described earlier, and obtained comparable results with the two methods. Beswick et al. (2008) found a median value of $q_{24} = 0.48$ for all sources, and a '*tentative deviation*' in the infrared / radio correlation at very low 24-μm flux densities, with the fainter sources having lower values of q_{24}. Fig. 11 shows all of the stacking results presented in this work, converted to a 1.4-GHz value where appropriate, along with those from Boyle et al. (2007) and Beswick et al. (2008). In order to display the data more clearly we focus on the 24-μm flux density range between 0.1 and 2 mJy.

There is a clear discrepancy between the results of Beswick et al. (2008), the xFLS results, and the results from the SWIRE surveys. The most noticeable effect is that the radio surveys with the lowest noise levels show the lowest values of q_{24} – the Beswick et al. (2008) survey is the deepest, at 3.6 μJy beam^{-1}, while the xFLS surveys are the next most sensitive, and the SWIRE fields are the least sensitive. However, the noise levels of the VLA xFLS survey (23 μJy beam^{-1}) and the ATCA CDFS sur-

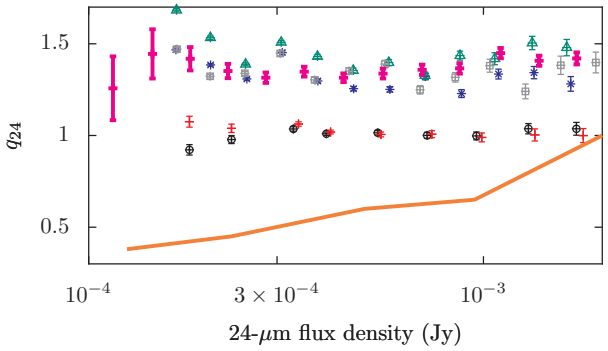

Figure 11. A comparison of all of the stacking results discussed in this work, using data shifted to 1.4 GHz where appropriate through the use of Equation 4 and $\alpha = 0.8$. The stacking results from this work are given by thin data points with error bars, with the VLA xFLS image (black circles), GMRT xFLS image (red upright crosses), GMRT ELAIS-N1 image (blue stars), GMRT ELAIS-N2 image (green triangles), and GMRT Lockman Hole image (grey squares) being shown, along with results from the Boyle et al. (2007) ATCA CDFS image (thick pink points; 'all-source' data) and the Beswick et al. (2008) MERLIN+VLA HDF-N image (thick orange solid line). All error bars represent the error on the median value of radio flux density.

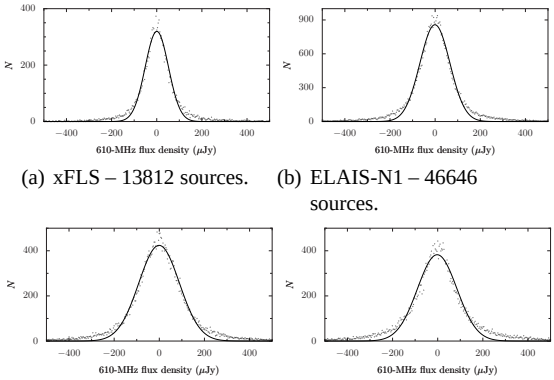

(a) xFLS – 13812 sources. (b) ELAIS-N1 – 46646 sources.

(c) ELAIS-N2 – 32265 sources. (d) Lockman Hole – 28042 sources.

Figure 12. Histograms of the flux density recorded within N random apertures in each of the 610-MHz surveys. No aperture correction factor has been applied to the measured flux densities.

vey (30 μJy beam^{-1}) are much more similar than the variation in noise between the 610-MHz xFLS and ELAIS-N2 images (30 μJy beam^{-1} and 80 μJy beam^{-1}), and yet the stacking results from those fields are still clearly inconsistent with each other, suggesting that this cannot be the only factor which is important.

In order to test whether the stacking results are being biased by the noise level of the radio image, the distribution of flux density within N random apertures was calculated for each of the GMRT images, and shown in Fig. 12. No aperture correction was applied to these flux density measurements, since applying the aperture correction only broadens each distribution by a factor of between 1.4 and 1.5, and does not affect the conclusions of this section. The slightly varying noise levels near to the edge of each image mean that a single Gaussian can not completely represent the flux density distribution, but there is no evidence for any asymmetry or significant non-Gaussianity in the measured values of flux density for any of the fields. The effects of noise on the stacking procedure will not systematically bias the measured values of radio flux density, and can not be responsible for the systematic difference in q'_{24} which is seen between fields.

There may be a significant number of radio-bright AGN in the HDF-N sample, which would lead to an decrease in q_{24}. Any AGN contamination would have to be large, since the 4.6 per cent of AGN sources within the ELAIS-N1 field made essentially no difference to the calculated value of q'_{24} in Section 3.2, and the median is naturally resistant to being affected by small numbers of outlier sources. All of the stacking studies presented here are infrared-selected, and the population would therefore be expected to be dominated by star-forming systems – this makes it unlikely, although not impossible, that large amounts of AGN contamination will be a problem. Biggs & Ivison (2006) have shown that the differential number counts of radio sources within the HDF-N are consistent with source counts from other deep observations – although this does not provide any information directly about the brightness of infrared-selected sources, it does show that the HDF-N is not an anomalously radio-bright region of sky.

80 per cent of the Beswick et al. (2008) sample are detected in the radio above 3σ, making it much more complete than the samples described in this work (the deepest of which has 2,558/14,820 = 17 per cent radio detections above 4σ). It is important to note that we have applied *no* radio detection criteria to the stacked samples (a major advantage of stacking experiments), so no bias should be entering the analysis through incompleteness – however, if the 'stacking bias' identified by White et al. (2007) did vary with flux density, or S/N, then a more incomplete sample may lead to a greater value of q_{24} being found. Either way, in order to change a value of $q_{24} = 0.48$ to 1.39 (from Beswick to Boyle) would require from Equation 3 that only 12 per cent of the true radio flux density was being measured by Boyle et al. (2007), while Beswick et al. (2008) were measuring the full value – it seems highly unlikely that such a large error could be occurring. There may be some stacking bias taking place, but we do not believe it can be responsible for the size of the observed difference between the Beswick et al. (2008) results and the other data. It would also not explain the difference between the essentially constant value of q_{24} found in this work and by Boyle et al. (2007), and the variation with 24-μm flux density found by Beswick et al. (2008).

The Beswick et al. (2008) sample is the only stacking study which is working with resolved radio sources – however, the flux density measurement method that they use should include all of the resolved flux density. Any loss of radio flux would lead to an increase in q_{24}, rather than the lower value that they find compared with other works.

None of the explanations for the discrepancy in stacking results are satisfactory – while we believe that the most likely explanation is some combination of an effect due to the differing noise levels and a stacking bias, this remains speculation. Nonetheless, all the indications are that the same effect is occurring equally to all radio sources in a field, and so while the absolute values of q_{24} and q'_{24} are uncertain, their dependence on infrared flux density will not be affected. We find no evidence for any variation in the value of q_{24} or q'_{24} over the 24-μm flux density range of 150-μJy and 10 mJy, and no evidence for a variation in the value of q'_{70} over the 70-μm flux density range 10 – 100 mJy.

5 CONCLUSIONS

We have compared the two methods commonly used in stacking experiments, and demonstrated that they give comparable measurements of the average radio flux density for binned sources. We have shown that the median flux density is a much more reliable estimator than the mean, and that the noise level of stacked images decreases as $1/\sqrt{N}$, at least until a depth of ~ 0.5 μJy beam^{-1} at 1.4 GHz. Creating stacked images leads to less information being retained on the flux density distribution of sources, and we argue that future stacking experiments should not make images, but instead work directly from the individual flux density measurements that can be calculated at each source position.

We have calculated q_{24} and q'_{24} from sources within the xFLS field, and demonstrated that they can be related to each other with the simple assumption that all radio sources have the spectral index of $\alpha = 0.4$, over the 24-μm flux density range of 150 μJy – 10 mJy. Using this conversion, we have compared the stacking results of Boyle et al. (2007) to the results obtained from our three SWIRE field images, and demonstrated that they are consistent, within the errors that can be placed on the median stacked values of q_{24}. There appears to be some field-to-field variation seen between the xFLS and SWIRE fields, with stacking results from the xFLS field leading to a value of q_{24} that is ~ 0.3 lower than the value seen in the SWIRE fields. This variation is also seen when stacking radio sources using the 70-μm catalogues of each field. Through comparison with the results of Appleton et al. (2004), who look at individual sources which are detected in the xFLS field, we conclude that our radio flux density measurements are not being significantly biased by the stacking procedure.

We have considered several potential explanations for the difference in the median values of q_{24}, and shown that effects such as a flux calibration error cannot be responsible for the difference in results. While we can not explain the systematic offset which is being seen, we believe that it originates in some combination of a 'stacking bias' and the varying noise levels of the different radio surveys. The systematic effect leads to an uncertainty in the absolute values of q_{24} and q_{70}, but not in their variation with infrared flux density.

We find no evidence for a variation in the median value of q_{24} from any of the survey fields down to a 24-μm flux density of 150 μJy. This is in agreement with the results of Boyle et al. (2007), although is in contrast to the tentative findings of Beswick et al. (2008). We find a similar result at 70 μm, although over the brighter flux density range of 10 – 100 mJy. We conclude that there is no evidence for any significant variation in the infrared / radio correlation with infrared flux density, down to the limits set by the extremely sensitive *Spitzer* observations of the xFLS and SWIRE fields.

ACKNOWLEDGMENTS

TG thanks the UK STFC for a Studentship. We thank the staff of the GMRT who have made these observations possible. The GMRT is operated by the National Centre for Radio Astrophysics of the Tata Institute of Fundamental Research, India.

REFERENCES

Afonso J., Mobasher B., Koekemoer A., Norris R. P., Cram L., 2006, AJ, 131, 1216
Appleton P. N., et al., 2004, ApJS, 154, 147
Becker R. H., White R. L., Helfand D. J., 1995, ApJ, 450, 559
Bertin E., Arnouts S., 1996, A&AS, 117, 393
Beswick R. J., Muxlow T. W. B., Thrall H., Richards A. M. S., Garrington S. T., 2008, MNRAS, 385, 1143
Biggs A. D., Ivison R. J., 2006, MNRAS, 371, 963
Boyle B. J., Cornwell T. J., Middelberg E., Norris R. P., Appleton P. N., Smail I., 2007, MNRAS, 376, 1182
Carilli C. L., et al., 2008, ApJ, in press (astro-ph/0808.2391v1)
Condon J. J., Cotton W. D., Yin Q. F., Shupe D. L., Storrie-Lombardi L. J., Helou G., Soifer B. T., Werner M. W., 2003, AJ, 125, 2411
de Jong T., Klein U., Wielebinski R., Wunderlich E., 1985, A&A, 147, L6
de Vries W. H., Hodge J. A., Becker R. H., White R. L., Helfand D. J., 2007, AJ, 134, 457
Fadda D., et al., 2006, AJ, 131, 2859
Fadda D., Jannuzi B. T., Ford A., Storrie-Lombardi L. J., 2004, AJ, 128, 1
Fazio G., et al., 2004, ApJS, 154, 10
Frayer D. T., et al., 2006, AJ, 131, 250
Garn T., Green D. A., Hales S. E. G., Riley J. M., Alexander P., 2007, MNRAS, 376, 1251
Garn T., Green D. A., Riley J. M., Alexander P., 2008a, MNRAS, 383, 75
Garn T., Green D. A., Riley J. M., Alexander P., 2008b, MNRAS, 387, 1037
Garn T., Green D. A., Riley J. M., Alexander P., 2009, in preparation
Garrett M. A., 2002, A&A, 384, L19
Helou G., Soifer B. T., Rowan-Robinson M., 1985, ApJ, 298, L7
Hodge J. A., Becker R. H., White R. L., de Vries W. H., 2008, AJ, 136, 1097
Ibar E., et al., 2008, MNRAS, 386, 953
Ivison R. J., et al., 2007, ApJ, 660, L77
Lacy M., et al., 2005, ApJS, 161, 41
Lonsdale C. J., et al., 2003, PASP, 115, 897
Murphy E. J., et al., 2006, ApJ, 638, 157
Norris R. P., et al., 2006, AJ, 132, 2409
Prandoni I., Gregorini L., Parma P., de Ruiter H. R., Vettolani G., Wieringa M. H., Ekers R. D., 2000, A&ASS, 146, 41
Rowan-Robinson M., et al., 2008, MNRAS, 386, 697
Roy A. L., Norris R. P., Kesteven M. J., Troup E. R., Reynolds J. E., 1998, MNRAS, 301, 1019
Sanders D. B., Soifer B. T., Elias J. H., Madore B. F., Matthews K., Neugebauer G., Scoville N. Z., 1988, ApJ, 325, 74
Shupe D. L., et al., 2008, AJ, 135, 1050
Sopp H. M., Alexander P., 1991, MNRAS, 251, 14P
Surace J. A., et al., 2005, The SWIRE Data Release 2: Image Atlases and Source Catalogs for ELAIS-N1, ELAIS-N2, XMM-LSS and the Lockman Hole, August 31, 2005 draft, available via `http://swire.ipac.caltech.edu/swire/astronomers/data_access.html`
Wals M., Boyle B. J., Croom S. M., Miller L., Smith R., Shanks T., Outram P., 2005, MNRAS, 360, 453
Werner M., et al., 2004, ApJS, 154, 1
White R. L., Helfand D. J., Becker R. H., Glikman E., de Vries W., 2007, ApJ, 654, 99
Yun M. S., Reddy N. A., Condon J. J., 2001, ApJ, 554, 803
Zheng X. Z., Bell E. F., Rix H.-W., Papovich C., Le Floc'h E., Rieke G. H., Pérez-González P. G., 2006, ApJ, 640, 784
Zheng X. Z., Dole H., Bell E. F., Le Floch'h E., Rieke G. H., Rix H.-W., Schiminovich D., 2007, ApJ, 670, 301

Zibetti S., White S. D. M., Schneider D. P., Brinkmann J., 2005, MNRAS, 358, 949